Final Draft
of the original manuscript:

Creep properties of different γ'- strengthened Co-base superalloys

A. Bauer[*1], S. Neumeier[1], F. Pyczak[2], R.F. Singer[3], M. Göken[1]

[1]Department of Materials Science & Engineering, Institute of General Materials Properties,
University Erlangen-Nürnberg, 91058 Erlangen, Germany

[2] Helmholtz-Zentrum Geesthacht, Centre for Materials and Coastal Research, 21502 Geesthacht, Germany

[3] Department of Materials Science & Engineering, Institute of Science and Technology of Metals,
University Erlangen-Nürnberg, 91058 Erlangen, Germany

alexander.bauer@ww.uni-erlangen.de, steffen.neumeier@ww.uni-erlangen.de, florian.pyczak@hzg.de, robert.singer@ww.uni-erlangen.de, mathias.goeken@ww.uni-erlangen.de

Abstract

The influence of various alloying elements on the creep properties of polycrystalline Co-base superalloys hardened by a ternary $L1_2$ compound, $Co_3(Al,W)$ (γ'-phase), was investigated. A Ti containing quaternary alloy shows creep strength similar to Ni-base superalloys IN100 and IN713C at 850 °C and strongly superior to conventional Co-base superalloys as Haynes 188. The activation energy for creep between 850 and 950 °C is similar to the polycrystalline Ni-base superalloy IN 100 in the same temperature range. Strengthening of the grain boundaries by third phase precipitates was found to be crucial for the mechanical properties. This can be achieved either by precipitation of borides or by additional intermetallic phases which precipitate due to oversaturation. During compressive creep at 850°C only a slight tendency for directional coarsening occurs, while at 950°C distinct γ/γ′-rafts perpendicular to the external compressive stress axis are formed which indicate a positive lattice misfit even at 950°C.

---

* Corresponding author. Tel: +49 9131 85 27485, fax: +49 9131 85 27504

Introduction

The need for high efficiency turbine engines leads to an increasing demand for materials capable to withstand high mechanical loads at elevated temperatures. Over the years, Ni-based superalloys became the most suitable materials for such purpose due to excellent high temperature strength provided by the two phase γ/γ′-microstructure [1, 2]. Consisting of a A1 matrix (γ-phase) and L1$_2$ ordered intermetallic compound (γ′-phase), such a microstructure also shows, in contrast to many other alloy systems, anomalous flow stress behavior [3]. Combined with sufficient oxidation resistance, such Ni-based superalloys offer a unique set of properties making it the material of choice for turbine discs and blades [1]. Conventional Co-based superalloys are utilized mostly in mechanically low loaded parts since they lack the possibility of γ′-strengthening at temperatures above 900 °C [1]. However, recently, Sato et al. [4] discovered a ternary intermetallic compound Co$_3$(Al,W) with a L1$_2$ structure, which showed for the first time the possibility of γ/γ′-strengthening in Co-based alloys. The lattice misfit of this new compound at elevated temperatures is significantly lower than of the L1$_2$ Co$_3$Ti phase [5, 6], which is not suitable for γ/γ′-strengthening. Suzuki et. al. reported the occurrence of a flow stress anomaly analogous to Ni-based alloys for Co-9Al-9W [7, 8] and showed that Ta increases the flow stress at the peak temperature. Shinagawa et al. [9] showed that additions of boron effectively strengthen the grain boundaries, thus improving the ductility of polycrystalline Co-9Al-9W alloy. First creep results [10] revealed that the γ′-strengthened polycrystalline Co-9Al-9W-0.12B alloy (at.%, as all other contents in this work) exhibits similar creep strength as the commercial Ni-based alloy IN 713C. In this work, the results of creep experiments on different polycrystalline alloys performed at temperatures between 850 °C and 950 °C are discussed. Furthermore, first creep tests on single crystalline Co-9Al-9W are described. The microstructure and dislocation arrangements in crept specimens are investigated with TEM.

Experimental procedure

The γ/γ′ Co-base superalloys investigated in this study were vacuum arc melted as cigar shaped specimens with a length of about 70 mm in a water cooled Cu mold. Casting porosity was checked by optical microscopy and found to be around 0.7 vol % for the investigated alloys. The typical grain size is approximately 250 μm. The nominal compositions are given in Table 1. Compositions of the conventional superalloys are given in Table 2. Additionally, results of EDS measurements are also provided, since certain deviations from the nominal composition occur as a result of insufficient melting due to the high melting point of tungsten and evaporation of Al. Complementary, glow discharge optical emission spectroscopy (GDOES) was utilized to confirm the boron content of the master alloys which are not measurable by EDS. Also, the silicon content in the Si-containing alloys had to be confirmed by GDOES due to overlapping element lines of Si and W in the EDS. For calibration a sample with a known Si content (8W-2Ta-2Si) determined by EPMA was utilized. GDOES measurements were conducted on a RF GD Profiler (HORIBA Jobin Yvon) equipped with a 4-mm-diameter anode operating at a radio frequency of 13.56 MHz and a power of 50 W. High-purity argon (99.9999 %) was used as a discharge gas at a pressure of 700 Pa.

Single crystal specimen was cast in a Bridgeman vacuum investment casting unit as a cylindrical bar with a diameter of 12 mm and a length of 85 mm. The melt was homogenized for 5 minutes at 1560 °C and then cast into the 1550 °C preheated mold. The SX casting mold was mounted on top of a water-cooled copper chill plate. The working pressure of the casting unit was 10^{-3} mbar. The withdrawal rate during solidification was 3 mm/min.

The heat treatment procedure consisted of a solution heat treatment at 1300 °C for 12 h in an argon atmosphere and aging at 900 °C for 200 h in air. The transformation temperature was measured by DSC with a sample of about 300 mg mass performed with a heating/cooling rate of 5K min^{-1} using a Netzsch STA 409 CD. Heat treatments of conventional alloys are as follows: Haynes188 - heat treatment at 1175 °C for 6 h; IN100 – solution heat treatment for 4 h at 1205 °C, aging for 4 h at 1080 °C and 8 h at 900 °C. IN713C was investigated in as cast condition since this is the usual condition for high temperature applications.

Characterization of the microstructures was conducted on a Zeiss Crossbeam 1540 EsB focused ion beam instrument with an Oxford Instruments EDS system. After mechanical polishing the samples were etched with 100 ml of distilled water, 100 ml of 32 % HCl, 10 ml of 65 % HNO_3 and 0.3 ml of Dr. Vogel's Spar etchant consisting of 30 % - 50 % 1-methoxy-

2-propanol and 2.5 % - 5 % thiocarbamide. Additionally, the microstructure of some samples was investigated by electron probe microanalysis (EPMA) on a JCXA 733 (JEOL).

Creep experiments in compression mode were performed at a constant applied stress ranging from 250 MPa to 500 MPa in air with temperatures between 850 °C and 950 °C. Cylindrical creep specimens with a height of 7.5 mm and a diameter of 5 mm were produced by electro-discharge machining. The maximum plastic strain in the creep tests was about 5 %. Microstructural investigations and density measurements (Archimedes' principle) revealed no cavities in the samples.

TEM investigations were performed on mechanically ground specimens taken perpendicular to the externally applied stress axis, which were subsequently thinned to electron transparency by electro twin jet polishing using a perchloric acid butanol electrolyte. For the investigation a Philips CM200 transmission electron microscope operated at 200 kV acceleration voltage was used.

Microstructural investigations

Microstructural investigations revealed that all alloys exhibit the γ/γ′-microstructure similar to that of Ni-base superalloys. SEM micrographs of selected alloys are shown later in Figure 9. The composition of the investigated alloys along with the corresponding γ′-volume fraction and transformation temperatures are given in Table 1. For alloys which possess additional intermetallic phases two values for the γ′-volume fraction are given. $V_f^{\gamma'/(\gamma,\gamma',IP)}$ is the γ′-volume fraction if all phases are taken into account, while $V_f^{\gamma'/(\gamma,\gamma')}$ indicates the γ′-volume fraction if only the phases γ and γ′ are considered. Some of the data shown here were already published in [10] in terms of microstructural investigation, but for easier comparison the whole data set is shown in Table 1.

Grain boundary precipitates morphology of boron-containing samples

The base alloy Co-9Al-9W consists of only two phases: the γ-matrix and the γ′-phase [4]. Addition of boron leads to the formation of borides along the grain boundaries as seen in Figure 1a and 1b, with a volume fraction being less than 1% as determined by stereographic methods. Also a γ′-depleted zone with a width of about 2 μm is discernable at the grain boundary.

The borides seem to be stable at 900 °C as they are still present after aging for 1000 h at 900 °C (Figure 1f), however, the width of the γ′-depleted zone has slightly increased. In Ni-

base alloys similar zones including carbides were already reported by the group of Nembach [11, 12], exhibiting a strength reducing effect if the width of the γ′-depleted zone exceeds a certain value. They found that this γ′-depletion occurs due to the titanium diffusion to the grain boundaries with the width w being a linear function of $t^{1/2}$ and having a saturation value. Thus, in case of the alloys investigated in this work, γ′-depletion occurs since tungsten, which is essential for the formation of the $L1_2$ phase, diffuses towards the grain boundaries to form borides. The evaluation of the width of the γ′-depleted zone as a function of $t^{1/2}$ on samples aged at 900 °C for 10, 50, 200 and 1000 h shows the same linear dependence on $t^{1/2}$ (Figure 2a) as found by Nembach.

The morphology of the borides at the grain boundaries does not change significantly with varying boron content, since the thickness of the borides and the γ′-depleted zone is nearly constant at equal heat treatment conditions (Figure 2b). However, the precipitation of borides takes place not only at the grain boundary, but also in its vicinity or inside the grains as small needles and occurs more frequent as the boron content increases (Figure 1b).

Samples with 0.04 at.% boron and additional 1 at.% Mo or 2 at.% Cr or V exhibit similar borides at the grain boundaries (the 9W-1Mo-0.04B sample is shown in Figure 1c). Thus these elements do not affect the solubility of boron in the alloy. However, boron-containing (0.04 - 0.08 at.%) samples with additions of 2 at.% Ti or Ta do not show any grain boundary precipitates possibly due to the higher solubility of boron in these alloys. Indeed, it is necessary to increase the boron content to 0.12 at.% to precipitate borides at the grain boundaries in a sample alloyed with 2 at.% Ti (see Figure 1d). However, such an increase in the boron content leads in the Ta-containing alloy to a different kind of precipitates at the grain boundaries as seen in Figure 1e. With the width of the precipitates being similar in size to that of the other boron containing alloys, no comparable γ′-depleted area has been developed even after aging for 200 hours at 900 °C. Only at a few areas a γ′-depleted zone is found. These microstructural differences seem to be a consequence of the higher formation enthalpy of Ta-borides compared to W-borides [13, 14]. Accordingly, Ta enriches at the grain boundary, which was found by EDX measurements, to form borides. W instead is still available for the formation of $Co_3(Al,W)$ precipitates and therefore no γ′ depletion occurs at the grain boundaries.

Grain boundary precipitates morphology of boron-free samples

The solubility for further alloying elements in the ternary alloy is quite different. The quaternary alloy with addition of 2 at.% Ta and reduction of the W content to 8 at.% [10] still

shows only the two-phase microstructure. Additions of 2 at.% of Ti or V, even with the W content of around 10 at.% [10] do not lead to other phases besides the γ- and γ′-phase. The same addition of Nb, however, leads to needle-like precipitates at the grain boundaries and inside the grains as seen in Figure 3a. Addition of 2 at.% Si to the ternary alloy leads to W rich precipitates at the grain boundaries with the morphology similar to those of the boron containing alloys. However, a Si or Nb content of 0.5 at.% is too low for the formation of such intermetallic phases. The addition of Mo was performed only on boron containing 9W alloy, thus, it is not clear whether the precipitates at the grain boundary were triggered by addition of B or Mo or a combination of both.

The addition of Ti, Nb, Si or Mo to the Ta containing alloy leads to quite different precipitate morphologies compared to the Ta-free alloys (Figure 3). While Ta has almost no influence on the precipitate morphology of the Ti or Nb containing alloy, the morphologies of the Si and Mo containing alloys changed considerably. Also the volume fraction (Vf) of the intermetallic phases (Figure 3) is by far higher than that in the other investigated alloys. According to the performed EPMA measurements, these intermetallic phases exhibit an increased content of W, Ta and Si or Mo, respectively.

A 5W2Ta2Mo alloy with a decreased W content of 5.5%, reported in [10], does not show any intermetallic phases possibly due to a lower supersaturation. Addition of 2 at.% Cr, V or Ir to the Ta containing alloy reported in [10] resulted as well in a γ/γ′ microstructure without any additional phases.

Creep strength

The results of the creep experiments of the investigated alloys will be firstly compared with conventional Co-base and Ni-base superalloys. Then, the influence of the boron content, addition of alloying elements along with the γ′-volume fraction and the precipitate morphology will be discussed in detail.

Comparison with conventional Co-base and Ni-base superalloys

Figure 4a shows creep curves of a boron-containing γ′-strengthened Co-base superalloy Co-9Al-9W-0.04B. Compared to the creep results of the conventional Co-base superalloy Haynes188, shown in Figure 4a, the γ′-strengthened alloy exhibits significantly improved creep strength. Haynes 188, like most conventional Co-base alloys do not possess a hardening intermetallic γ′-phase and benefits from solid solution and carbide hardening.

Figure 4b contains creep curves of the Ni-base superalloy IN713C and shows that the alloy Co-9Al-9W-0.04B exhibits comparable creep strength within the scatter range. The difference in the minimum creep rate within two polycrystalline samples of the same 9W-0.04B alloy are possibly due to slight differences in grain size or grain orientation. IN713C alloy was tested in as cast condition since heat treatment has no major improvement on the mechanical properties [15]. The as cast condition is the usual condition for an application of IN713C as a high temperature material.

For determination of the activation energy Q for creep, additional creep experiments were performed at three different temperatures (850, 900 and 950 °C) as seen in Figure 5.

According to the Norton creep law:

$$\dot{\varepsilon} = A \cdot \sigma^n \cdot \exp\left(-\frac{Q}{RT}\right) \tag{1}$$

with constant A, applied stress in compression σ, stress exponent n, activation energy Q, gas constant R and temperature T in Kelvin, the activation energy of the investigated alloys is about 740 kJ/mol in the given temperature range. This value is considerably higher than that reported for lattice diffusion in Co of 280 kJ/mol [16]. However, in polycrystalline Ni-base superalloys the situation is quite similar. The activation energy for lattice diffusion in Ni [16] is very close to that of Co and the activation energy of the γ′-hardened Ni-base superalloy IN 100 is also about twice as high (720 kJ/mol) in the temperature range from 900 °C to 975 °C [17] . This is significantly higher compared to the activation energy reported for the more complex single crystalline Ni-base superalloy CMSX-4 tested at 654 MPa between 800 °C and 950 °C [18].For a further comparison, the creep strength of polycrystalline Co-base superalloys 9W-B and 9W-2Ti-0.12B and Ni-base superalloys IN 713C and IN 100, tested under the same condition, are shown in Figure 6. The data on IN100 which is a typical polycrystalline Ni-base superalloy with a γ′-volume fraction of about 55% are in good agreement with the data published by Dennison et al. [17]. In comparison to alloy 9W IN 100 exhibits slightly higher creep strength. However, the creep strength of the investigated boron-containing Co-base superalloy with an addition of 2 at.% Ti is already superior. Although IN 100 possesses a lower density of 7.8 g/cm^3 compared to the investigated Co-base superalloys with a density in the range of 9.4 g/cm^3 – 10.2 g/cm^3, these results show obviously the potential of the Co-base superalloys since they are not yet as highly alloyed as their Ni-base counterparts and in their early stages of development.

7

Influence of boron content

Minor additions of boron lead to grain boundary strengthening with substantially improved creep strength comparable with the polycrystalline Ni-base superalloy IN713C. It seems that variations in the amount of boron do not influence the creep properties (stress dependence) at 850 °C as shown in Figure 7. At a load of 300 MPa and higher a clear minimum in the creep rate was reached at about 0.6%–0.8% plastic strain. At 250 MPa, however, no minimum was reached in some of the tests. Therefore, the data point which is marked with an arrow only gives an upper limit for the minimum creep rate.

The DSC measurements (Table 1) show that boron has also no influence on the liquidus temperature of the material; thus, the boron content can be adjusted according to its influence on other properties like the oxidation behavior [19, 20]. Creep data on a <100>-orientated single crystalline Co-9Al-9W sample are also shown in Figure 7; however, no improvement in creep strength is found at the test temperature. Nevertheless, the fact that a boron free single crystalline specimen exhibits the same creep strength as polycrystalline variants with added boron proofs that the reason for the improvement due to the addition of boron is really grain boundary strengthening. Indeed, the creep properties of a boron free polycrystalline alloy are significantly worse (Figure 7a).

However, the existence of grain boundary precipitates does not automatically provide sufficient grain boundary strength, since also samples with 0.04 at.% boron and additional 2 at.% Cr or V show decohesion of the grain boundaries at much earlier stages of plastic deformation than in case of other investigated alloys. The reason for this behavior is not understood, considering the fact that the alloys were melted from the same master alloy and the boron content was the same as that of alloy 9W-1Mo-0.04B. Samples with an addition of 0.04 at.% of boron and 2 at.% of Ta or Ti which do not show any grain boundary precipitates failed early in creep tests as well.

Influence of alloying elements and γ′ - volume fraction

A similar improvement in creep strength as by addition of boron can be achieved by addition of 2 at.% of Nb (Figure 8). In this case, formation of needle-like intermetallic phases at the grain boundaries (Figure 3a) prevents their decohesion during creep tests. 10W2Nb shows similar creep strength as the boron containing ternary alloys at lower stress levels, however, 10W-2Nb and 9W-B possess different stress exponents n (10W-2Nb: n=6; 9W-B: n=9.6), thereby 10W2Nb has better creep strength at higher stress levels (lower minimum strain rate). Figure 8 contains only data on experiments at 350 MPa. The complete stress range tested is

shown in Figure 12. The difference in the γ′-volume fraction (9W-B: 58% and 10W-2Nb: 81%) is also significant. Thus, it is actually open whether the increased creep strength of 10W2Nb is a result of the formation of additional intermetallic phases at grain boundaries, the increased γ′-volume fraction or a combination of both.

However, the optimum value for the γ′-volume fraction is known to be around 70 % for Ni-base superalloys [21]. Accordingly, it is assumed that this value is also an optimum for these γ′-hardened Co-base alloys. Indeed, the above mentioned 9W-2Ti-0.12B alloy with a γ′-volume fraction of about 73% (Figure 9a), exhibits not only a creep strength comparable to the Ni-base alloy IN 100 (Figure 6) but is also superior to all other alloys investigated in this work as seen in Figure 8.

The addition of Mo to the boron containing ternary alloy leads to a similar γ′-volume fraction of 72 % in alloy 9W-1Mo-0.04B (Figure 9b). However, as shown in Figure 8 and Figure 12, the creep strength of this alloy is only better at lower stresses due to the relatively high stress exponent. A possible explanation will be given later. The decreased creep strength of alloy 10W-2Si despite of a similar γ′-volume fraction of about 72 % (Figure 9c) indicates that Si decreases the creep strength.

According to the results of Suzuki et al. [8], Ta has a favorable influence on the flow stress. However, compared to the ternary boron-containing alloys, no significant increase in creep strength could be achieved possibly due to the high γ′-volume fraction of 82 %, which is beyond the optimum level. As shown in Figure 8 and Figure 12 the 9W-2Ta-0.12B alloy has similar creep strength and only slightly lower stress exponent as in the case of Mo-addition.

Creep experiments on Ta containing alloys with additional 2 at. % of Nb, Si or Mo showed in all cases inferior creep strength than that of the Ta free variants; see Figure 8. One possible reason might be again, the value of the γ′-volume fraction (Figure 8) being significantly different than the suggested 70 %. However, in case of the Nb addition, the volume fraction of the γ′-phase is slightly closer to the optimum value than in the 10W2Nb. Since the intermetallic phases at the grain boundaries as well as their volume fractions are very similar in both Nb containing alloys, the decreased creep strength could possibly result from the lower W content of the 8W2Ta2Nb alloy as the solid solution strengthening effect of W is reduced.

The reason for the decreased creep strength of the alloys containing Si and Mo can be the decreased microstructure stability as the volume fraction of additional intermetallic phases at the grain boundaries and inside the grains (besides γ and γ′) has substantially increased in the quinary alloys 8W-2Ta-2Si and 8W-2Ta-2Mo (Figure 3).

In alloy 8W-2Ta-2Si the volume fraction $V_f^{\gamma'/(\gamma,\gamma',IP)}$ of the γ′-phase is about 53 % taking all existing phases into account, since 13 % of the material consists of further intermetallic phases. This is much lower than in the 10W-2Si alloy. In case of alloy 8W-2Ta-2Mo the γ′-volume fraction $V_f^{\gamma'/(\gamma,\gamma',IP)}$ is approx. 76%, since 16 % of the material consists of further intermetallic phases. However, in the γ/γ′-regions, where no additional intermetallic phases are present, the γ′-volume fraction $V_f^{\gamma'/(\gamma,\gamma')}$ is nearly 91 % . This is too high for a reasonable strengthening since the deformation occurs mostly in the γ′-phase and the advantageous effect of the γ/γ′-interface gets lost [21].

Added elements have manifold impact on the properties important for creep strength. As long as the grain boundary strength is sufficient, the achieved creep strength is additionally influenced by the γ′-volume fraction, the lattice misfit and the induced coherency stresses, the diffusivity and solid solution hardening effect of the alloying element. Due to these various factors no distinct dependency between the γ′-volume fraction and the obtained creep strength is found.

SEM investigations of the γ/γ′-microstructure after the creep tests revealed no strong change in the morphology of the γ′-phase (e.g. rafting) at 850°C as shown in Figure 9. Only a slight tendency for directional coarsening is visible in images parallel and perpendicular to the external compressive stress axis. According to Reed [2], the test conditions of the experiments possibly predict the dominance of the tertiary creep regime with plastic deformation occurring mainly in matrix channels. Indeed, in first TEM investigations, ordinary dislocations of a/2 <101>{111} type were found in matrix channels perpendicular to the external compressive stress axis in alloy 9W-0.12B (Figure 10a). These dislocations are mainly arranged in structures which are similar to early stages of the build-up of interfacial dislocation networks at the γ/γ′-interfaces in Ni-base superalloys [22]. Additionally, some γ′-precipitates are sheared by stacking faults (marked by arrows in Figure 10a), which extend also over the matrix channels and continue over the neighboring γ′-precipitates. While further investigations are necessary one can already speculate that an increasing dislocation density in the matrix channels leads to hardening in these regions. This would explain the pronounced decrease in creep rate during primary creep. A similar steep drop in creep rate during the primary stage was theoretically predicted and experimentally evidenced by Svoboda and Lucas for the Ni-base SX-alloy CMSX-4 at 1000 °C [23]. In [23] the plastic deformation in matrix channels was identified as reason for this as also discussed for 9W-0.12B here.

In comparison, alloy 10W-2Nb exhibits a rather different deformation structure at 850°C. Here mainly stacking faults shearing γ'-precipitates are found while no dislocation activity in the matrix channels is present as is clearly visible in Figure 10b. This difference in the deformation structure between alloys 9W-0.12B and alloy 10W-2Nb can either stem from the addition of niobium or from the higher γ'-volume fraction of 81 % in 10W-2Nb compared to 58 % in alloy 9W-0.12B.

Due to the high γ'-volume fraction the matrix channels in alloy 10W-2Nb are rather narrow with the associated high Orowan stresses, which probably make dislocation generation in the matrix channels unfavorable compared to shearing of γ'-particles. Already from this limited observations it can be deduced that the deformation and creep mechanisms differ significantly between alloys 9W-0.12B and 10W-2Nb as the observed dislocation and fault structures are different. Nevertheless, to fully clarify this, further investigations on the deformation structures and creep mechanisms especially in high γ'-volume fraction alloys similar to 10W-2Nb are necessary, which are beyond the scope of this paper.

At higher temperatures, T = 950°C, the microstructure of alloy 9W-0.08B has changed significantly during creep in contrast to that at 850°C (compare Figure 11 and Figure 9). Obviously, the γ'-volume fraction is much lower as the creep temperature is close to the γ'-solvus temperature of 984°C (see Table 1). Additionally, γ/γ'-rafts are formed perpendicular to the compressive stress axis in grains which [001] orientation is parallel to the stress axis as shown in Figure 11b. This indicates that the lattice misfit of the ternary alloy 9W-0.08B is not only positive at room temperature, as found in a similar ternary Co-base superalloy by Sato et al. [4], but also at 950°C [2]. Additionally, it should be noted that in grains with other orientations such a directional coarsening does not necessarily occur (Figure 11a).

In summary, this difference in microstructural evolution between 850 °C and 950 °C, i.e. no or only slight directional coarsening and strong rafting, respectively, shows that also in γ/γ'-Co-base superalloys, similarly to Ni-base superalloys, 850 °C is too low for rafting to occur and higher temperatures of 950 °C are needed [2].

Influence of grain boundary precipitate morphology

During the creep experiments it became clear that the precipitate type and its morphology have a substantial impact on the value of the stress exponent *n* (see eq. (1)). From the investigations on the stress exponent, two groups can be identified (Figure 12). The alloys 10W-2Nb, 8W-2Ta-2Nb, 8W-2Ta-2Mo and 8W-2Ta-2Si exhibit lower *n* values of 6 to 7.7 (Figure 12a). These alloys have in common the presence of intermetallic phases at the grain

boundary which are, with the exception of 8W-2Ta-2Si, needle-like in structure as seen in Figure 3 and penetrate the adjacent grains. The precipitates in 8W-2Ta-2Si have a rather round shape, however, the grain boundaries are quite serrated. Both precipitate morphologies lead to a high grain boundary strength leading to the value of the minimum strain rate being less sensitive to stress changes as in case of the other alloys.

The second group of alloys consists of the boron-containing ternary alloys 9W-xB, alloys 10W-2Si and 9W-2Ti-0.1B. They exhibit higher n values in the range between 9.2 and 10.8 (Figure 12b). Only the grain boundaries of these alloys are saturated with a small fraction of W-containing precipitates within a γ′-depleted area as discussed previously. The higher n-values indicate a reduced creep strength at higher loads. A possible explanation for such a behavior is the influence of the γ′-depleted zone near the grain boundary on the mechanical properties as reported by Nembach [11, 12]. They investigated the influence of the widths of the γ′-depleted zones on the mechanical properties of polycrystalline Ni-base superalloy NIMONIC PE16 and found that wide γ′-depleted zones reduce quite strongly the yield strength. Due to compatible deformation of neighbouring grains dislocations are formed in the soft γ′-depleted zone and emitted towards the γ′-strengthened interior of the grains where they pile up. The ease with which dislocations are generated in the γ′-depleted zone and the ensuing dislocation pile-ups lead to softening of the material [11, 12]. Such wide and soft γ′-depleted zone, which are present also in the alloys of the second group and comparable in size due to the same aging time, seem to reduce also the creep strength at high stresses. Additionally, in contrast to the alloys of the first group, which do not possess such wide γ′-depleted zones, no penetration of the adjacent grains by the precipitates occurs. However, at lower loads these alloys seem to have better creep strength than the alloys of the first group, since no depletion on solid solution strengthening elements occurs as the volume fraction of the intermetallic phases at the grain boundaries is limited and the grain boundary strength becomes less crucial.

The 9W-1Mo-0.04B alloy with its stress exponent of 17.6 can be assumed as an extreme case of the second group (Figure 12b), since it exhibits similar precipitates at the grain boundaries. However, in the case of the Mo-containing alloy the grain boundaries are relatively straight in comparison to the alloys of the second group; see Figure 3d. This eases grain boundary decohesion when the externally applied stress overcomes the grain boundary strength. The 9W-2Ta-0.12B alloy possessing a high stress exponent of 14.5 can be treated as another extreme case. The grain boundaries are quite straight as well, however, with no serrations

present similar to the 9W-1Mo-0.04B alloy and without the γ′-depleted area near the grain boundary.

Conclusions

1. The creep strength of boron containing γ′-strengthened Co-base superalloys is comparable to Ni-base superalloy IN713C. Boron containing ternary alloy with addition of 2 at. % Ti exhibited even better creep strength, comparable with the Ni-base alloy IN100. Varying amount of boron has no influence on the morphology of the grain boundary precipitates, on the width of the γ′-depleted zone, on the creep strength as well as on the phase transformation temperatures of the ternary alloys.

2. In boron free alloys, the formation of intermetallic phases at the grain boundary can have a strengthening effect as well. A Nb containing alloy exhibited a creep strength comparable with a boron containing ternary alloys. However, an excessive volume fraction of intermetallic phases in Ta-containing alloys with additions of Si or Mo leads to a severe drop in the creep strength.

3. The morphology of the grain boundary precipitates determines the grain boundary strength, thus has a strong impact on the stress exponent.

4. From creep tests at different temperatures the activation energy for creep has been determined to be around 740 kJ/mol, similar to polycrystalline Ni-base superalloy IN 100.

5.   At 850°C no or only slight directional coarsening occurs, while during compressive creep at 950°C γ/γ′-rafts perpendicular to the external compressive stress axis are formed which indicate a positive lattice misfit even at 950°C.

Acknowledgements

References

[1] C. T. Sims, N. S. Stoloff, and W. C. Hagel. *Superalloys II*. John Wiley & Sons, New York, United States of America, 1987.

[2] R. C. Reed. *The Superalloys*. Cambridge University Press, Cambridge, United Kingdom, 2006.

[3] R.G. Davies and N. S. Stoloff. *Transactions of the Metallurgical Society of AIME*, 233:714–719, 1965.

[4] J. Sato, T. Omori, K. Oikawa, I. Ohnuma, R. Kainuma, and K. Ishida. *Science*, 312:90–91, 2006.

[5] C. Rogister, D. Coutsouradis, and L. Habraken. *Cobalt*, 34:3–8, 1967.

[6] P. Viatour, J.M. Drapier, and D. Coursouradis. *Cobalt*, 3:67–74, 1973.

[7] A. Suzuki, G. C. DeNolf, and T. M. Pollock. *Scripta Materialia*, 56(5):385 – 388, 2007.

[8] A. Suzuki and T. M. Pollock. *Acta Materialia*, 56(6):1288 – 1297, 2008.

[9] K. Shinagawa, T. Omori, K. Oikawa, R. Kainuma, and K. Ishida. *Scripta Materialia*, 61(6):612 – 615, 2009.

[10] A. Bauer, S. Neumeier, F. Pyczak, and M. Göken. *Scripta Materialia*, 63(12):1197 – 1200, 2010.

[11] R. Maldonado and E. Nembach. *Acta Materialia*, 45(1):213 – 224, 1997.

[12] T. Krol, D. Baither, and E. Nembach. *Acta Materialia*, 52(7):2095 – 2108, 2004.

[13] V.G. Kudin and V.A. Makara. *Inorganic Materials*, 38(3):216–219, 2002.

[14] A. N. Kolmogorov and S. Curtarolo. *Physical Review B - Condensed Matter and Materials Physics*, 74(22), 2006.

[15] J. R. Brinegar, J. R. Mihalisin, and J. Vadersluis. *Superalloys*, pages 53–62, 1984.

[16] O.D. Sherby and J. Weertman. *Acta Metallurgica*, 27(3):387 – 400, 1979.

[17] J.P. Dennison, P.D. Holmes, and B. Wilshire. *Materials Science and Engineering*, 33(1):35 – 47, 1978.

[18] J. Svoboda and P. Lukas. *Materials Science and Engineering: A*, 234-236(0):173 – 176, 1997.

[19] L. Klein, A. Bauer, S. Neumeier, M. Göken, and S. Virtanen. *Corrosion Science*, 53(5):2027 – 2034, 2011.

[20] L. Klein, Y. Shen, M.S. Killian, and S. Virtanen. *Corrosion Science*, 53(9):2713 – 2720, 2011.

[21] T. Murakumo, T. Kobayashi, Y. Koizumi, and H. Harada. *Acta Materialia*, 52(12):3737 – 3744, 2004.

[22] R.D Field, T.M. Pollock, and Murphy W.H. *in S.D. Antolovich, R.W. Stusrud, R.A. MacKay, D.L. Anton, T. Khan, R.D. Kissinger, D.L. Klarstrom, eds, Superalloys 1992 (Warrendale, PA: The Metallurgical Society of AIME,1992)*, pages 557–566.

[23] J. Svoboda and P. Lukas. *Acta Materialia*, 46(10):3421 − 3431, 1998.

[24] Bieber et al. High temperature alloys and articles, US patent 2.570.193, Oct. 9, 1951.

[25] Haynes 188 alloy. Haynes International, Inc.

Table 1: Investigated alloys. The composition was measured on the solution heat treated samples by EDS. See also [10]. (Compositions marked with "*" could not be determined using EDS. However, GDOES measurements confirmed the nominal Si content.). Values for the γ′ volume fraction marked with ** represents the γ′-volume fraction if all phases are taken into account $V_f^{\gamma'/(\gamma,\gamma',IP)}$, while the γ′-volume fraction $V_f^{\gamma'/(\gamma,\gamma')}$ indicates the γ′-volume fraction if only the phases γ and γ′ are considered.

Utilized abbreviations	Nominal composition	Measured composition / at. %					Transformation temperatures / ° C			γ′ volume fraction /%
		Co	Al	W	Ta	X	Solv	Solid	Liq	$V_f^{\gamma'/(\gamma,\gamma')}$
9W	Co-9Al-9W	83.4	8.1	8.4	-	-	963	1445	1469	58
9W(SX)	Co-9Al-9W	81.8	8.5	9.6	-	-	985	1441	1466	58
9W-0.04B	Co-9Al-9W-0.04B	81.9	8.4	9.7	-	-	986	1440	1467	58
9W-0.08B	Co-9Al-9W-0.08B	81.5	8.9	9.5	-	-	984	1439	1465	58
9W-0.12B	Co-9Al-9W-0.12B	82.2	8.3	9.4	-	-	982	1444	1469	58
8W-2Ta-0.08B	Co-9Al-8W-2Ta-0.08B	80.4	8.9	8.5	2.2	-	1101	1414	1439	80
9W-2Ta-0.12B	Co-9Al-9W-2Ta-0.12B	79.8	8.9	9.3	2.0	-	1097	1410	1434	82
8W-2Ta-2Nb	Co-9Al-8W-2Ta-2Nb	82.6	8.0	6.7	1.4	1.4	1079	1390	1411	78
9W-0.5Nb	Co-9Al-9W-0.5Nb	82.0	8.2	9.4	-	0.4	1011	1430	1459	72
10W-2Nb	Co-9Al-10W-2Nb	78.6	9.4	10.2	-	1.8	1064	1377	1426	81
9W-1Mo-0.04B	Co-9Al-9W-1Mo-0.04B	81.2	8.2	9.4	-	1.1	994	1436	1461	72
8W-2Ta-2Mo	Co-9Al-8W-2Ta-2Mo	78.5	8.2	9.6	1.8	1.8	1082	1398	1417	91/76**
10W-0.5Si	Co-9Al-10W-0.5Si	81.5	8.4	10.1	-	0*	989	1434	1462	65
10W-2Si	Co-9Al-10W-2Si	81.0	8.7	10.3	-	0*	998	1415	1449	72
8W-2Ta-2Si	Co-9Al-8W-2Ta-2Si	81.2	8.1	7.7	1.6	1.8	1054	1392	1413	61/53**
8W-2Ta-2Ti	Co-9Al-8W-2Ta-2Ti	79.2	7.6	9.2	1.9	2.1	1153	1392	1411	92
9W-2Ti-0.04B	Co-9Al-9W-2Ti-0.04B	80.9	7.9	9.1	-	2.1	1075	1413	1438	73
9W-2Ti-0.12B	Co-9Al-9W-2Ti-0.12B	79.8	8.4	9.6	-	2.2	1080	1414	1434	75
9W-2V-0.04B	Co-9Al-9W-2V-0.04B	80.7	8.0	9.3	-	2.1	1016	1430	1456	82
9W-2Cr-0.04B	Co-9Al-9W-2Cr-0.04B	80.5	8.1	9.4	-	2.0	975	1439	1464	63

Table 2: Reference alloys. Compositions are given in atomic percent.

Alloy	Ni	Co	Cr	Mo	W	Al	Ti	Nb	Fe	Mn	Si	C	B	Zr	La
IN 100 [2]	56.8	13.8	10.4	1.7	-	11.0	5.3	-	-	-	-	0.8	0.07	0.04	-
IN 713C [24]	69.1	-	13.2	2.4	-	12.4	0.9	1.3	-	-	-	0.5	0.06	0.06	-
Haynes188 [25]	23.4	39.4	26.4	-	4.7	-	-	-	3.3	1.4	0.8	0.5	0.09	-	0.01
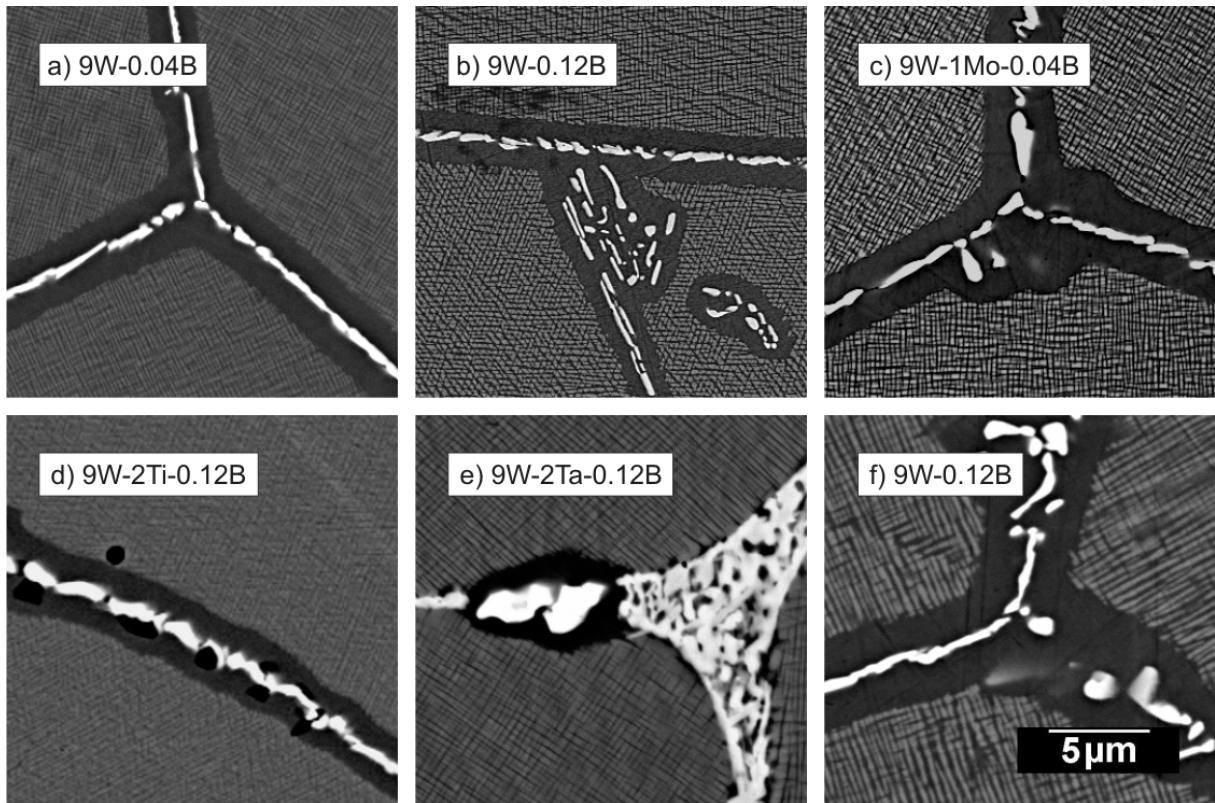
Figure 1: Morphology of the grain boundaries of the alloys with different boron content. a-e) Heat treatment 12 h at 1300 °C and 200 h at 900 °C. The volume fraction of the grain boundary phase is less than 1%. f) The 9W-0.12B alloy also has been investigated after a heat treatment of 12 h at 1300 °C and 1000 h at 900 °C. All micrographs in this figure have the same magnification.
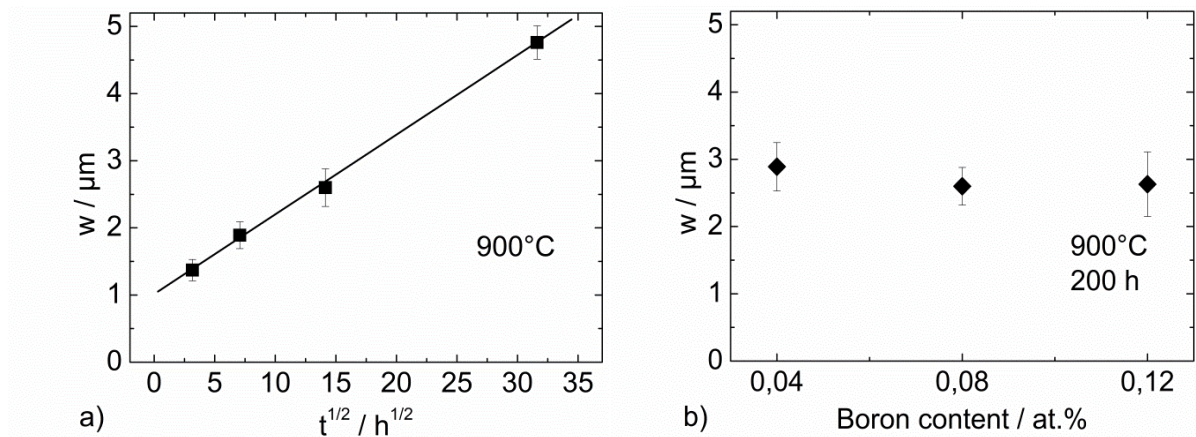
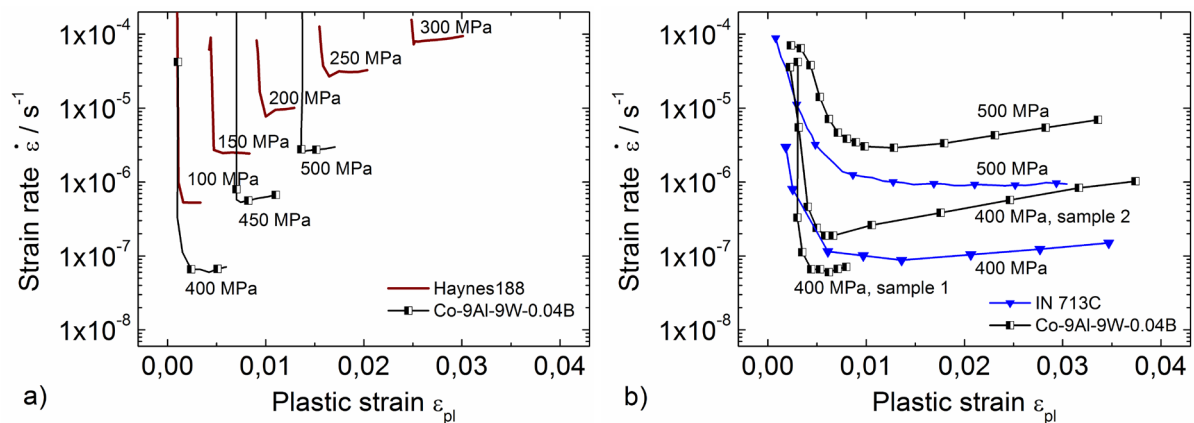**Figure 2: Width of the γ'-depleted zone as a function of $t^{1/2}$ (a) and as a function of the boron content (b).**
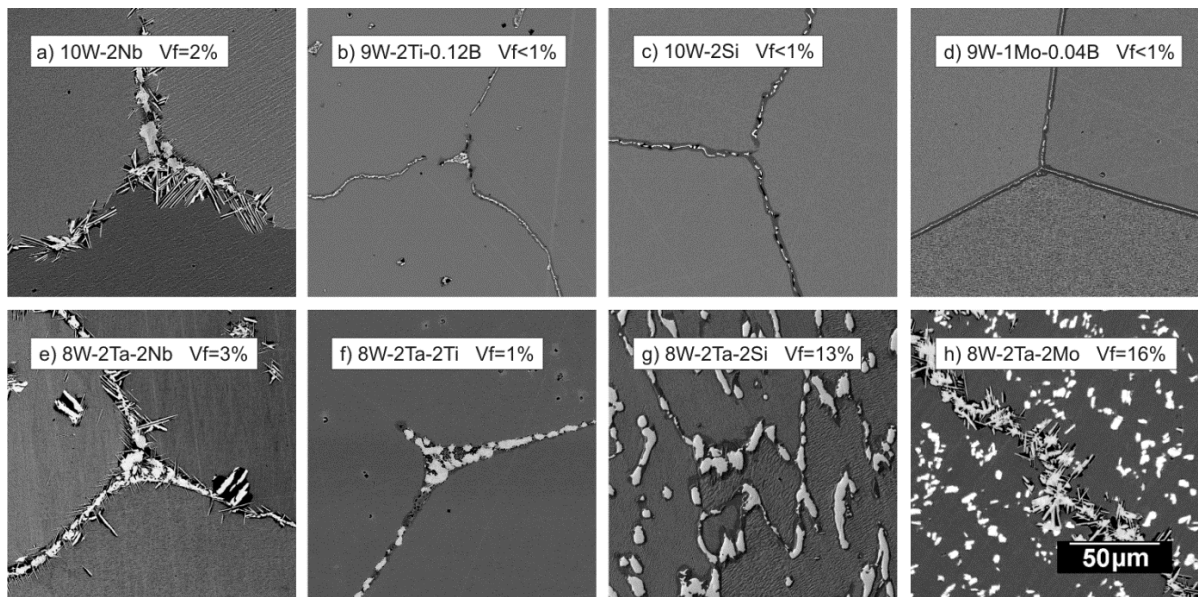
Figure 3: Influence of the Ta addition on the grain boundary morphology. Upper row: alloys without Ta; lower row: alloys with Ta. (Vf = volume fraction; heat treatment: 12 h at 1300 °C and 200 h at 900 °C). All micrographs in this figure have the same magnification.

Figure 4: Creep curves of experiments performed at 850 °C with several stress changes. The applied stresses in MPa are indicated next to the creep curves. a) Creep experiments on alloy Co-9Al-9W-0.04B and a conventional Co-base alloy Haynes188. b) Creep experiments on Co-9Al-9W-0.04B and Ni-base IN713C. At a stress of 400 MPa two different curves are shown to indicate the scatter width.
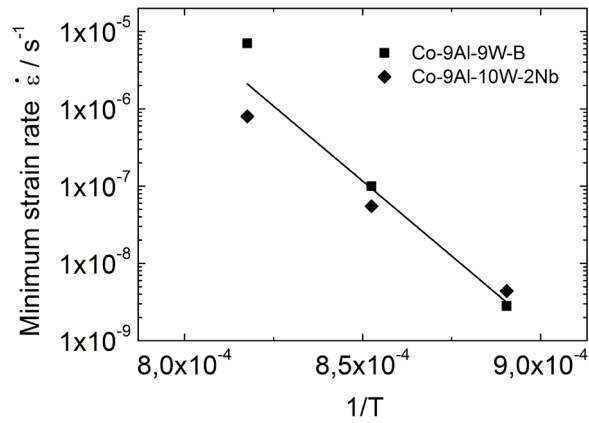
Figure 5: Minimum creep rate plotted over inverse temperature for creep experiments performed at 850 °C, 900 °C and 950 °C at a stress level of 250 MPa.
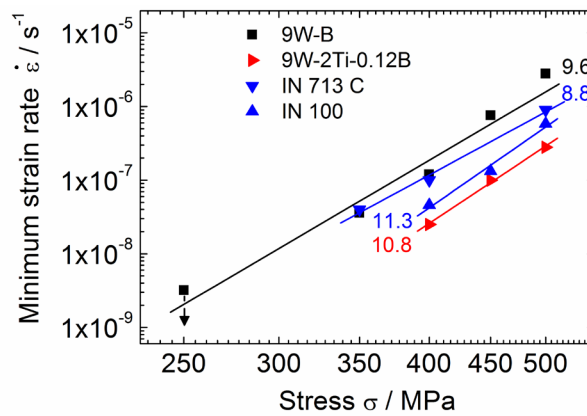
Figure 6: Comparison of creep strength of polycrystalline Co-base (9W-B and 9W-2Ti-0.12B) and Ni-base superalloys (IN 100 and IN 713 C) tested at 850 °C at different stresses. The corresponding stress exponent n is shown next to the respective line.
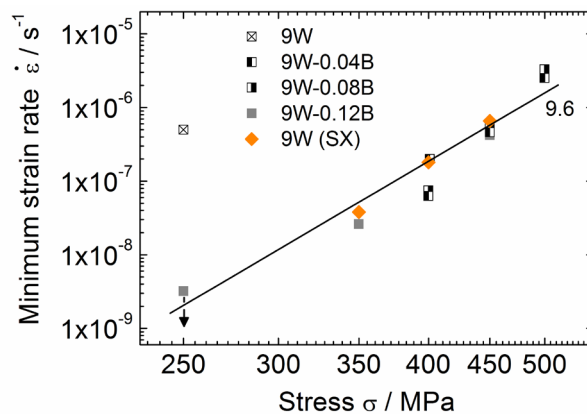

Figure 7: Norton plot of polycrystalline alloys with different boron contents and the single crystalline ternary alloy 9W (SX) creep tested at 850 °C and different stresses.
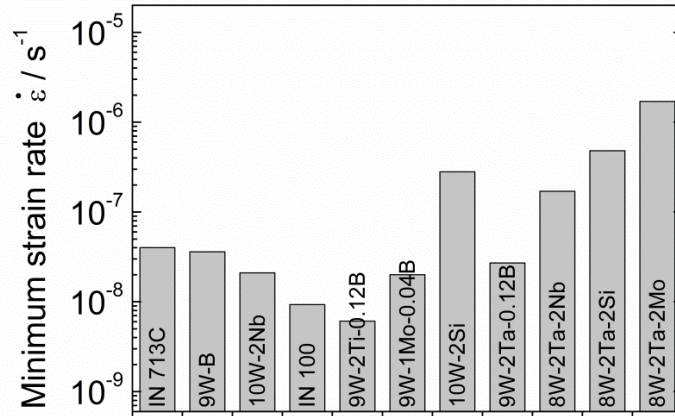
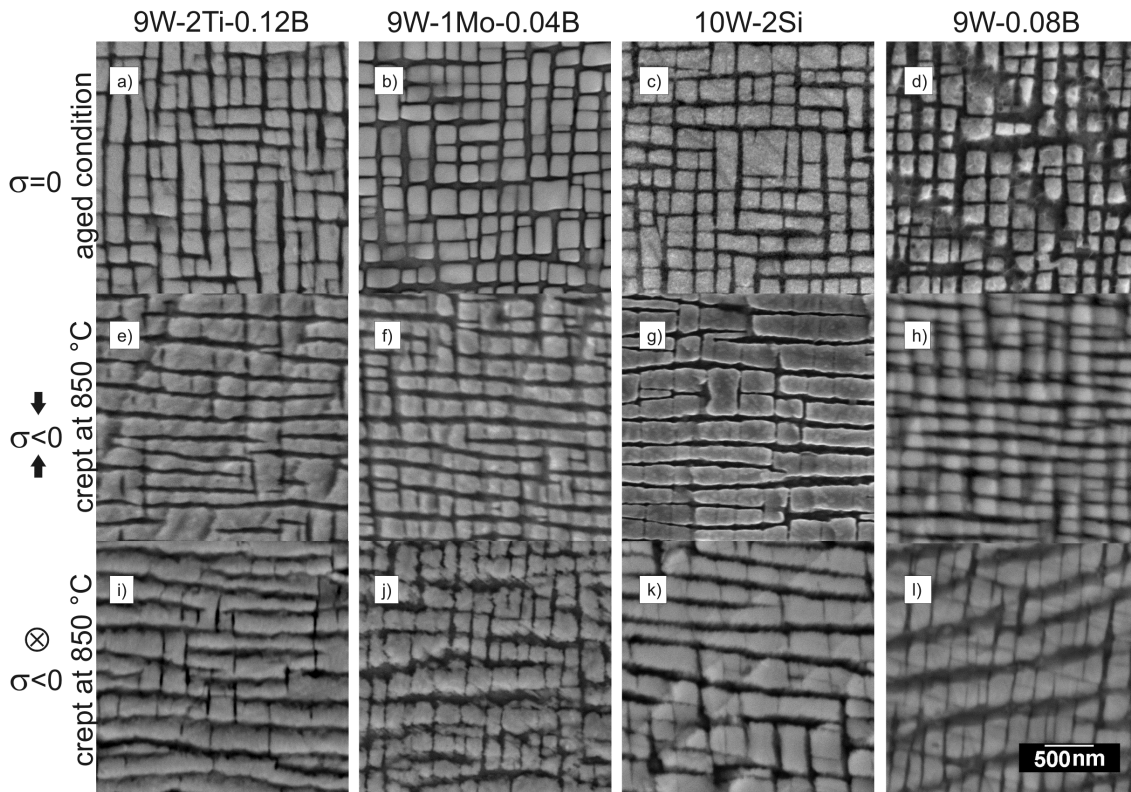**Figure 8: Creep experiments on the investigated alloys at 850 °C. Only minimum creep rates at 350 MPa are shown.**
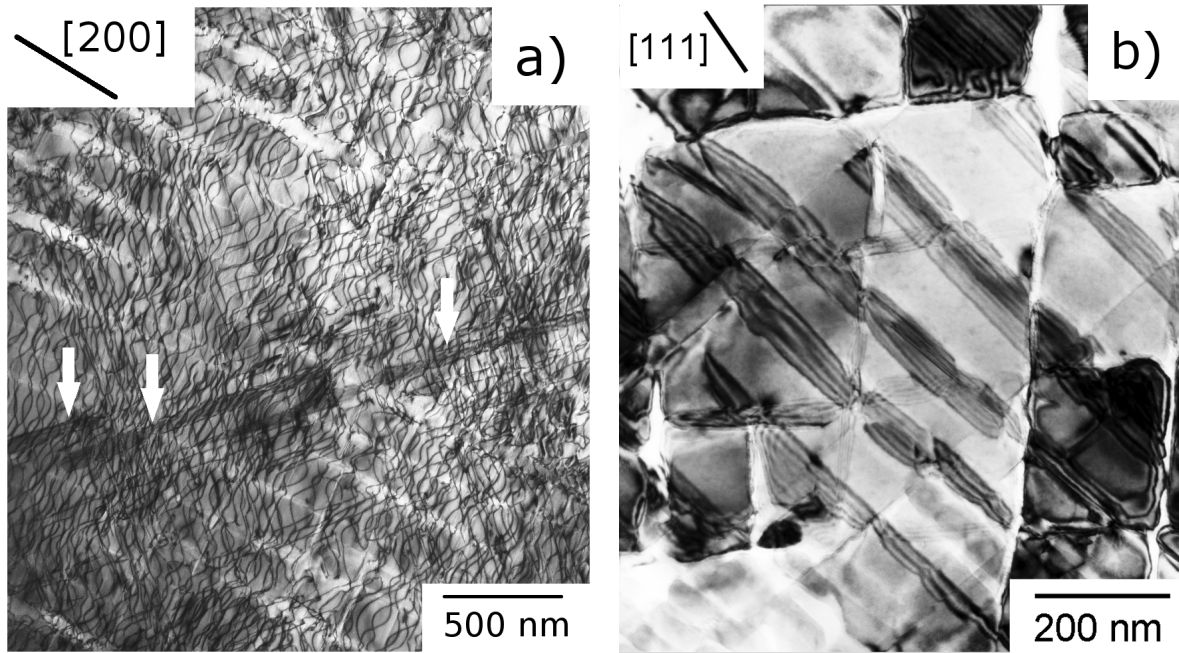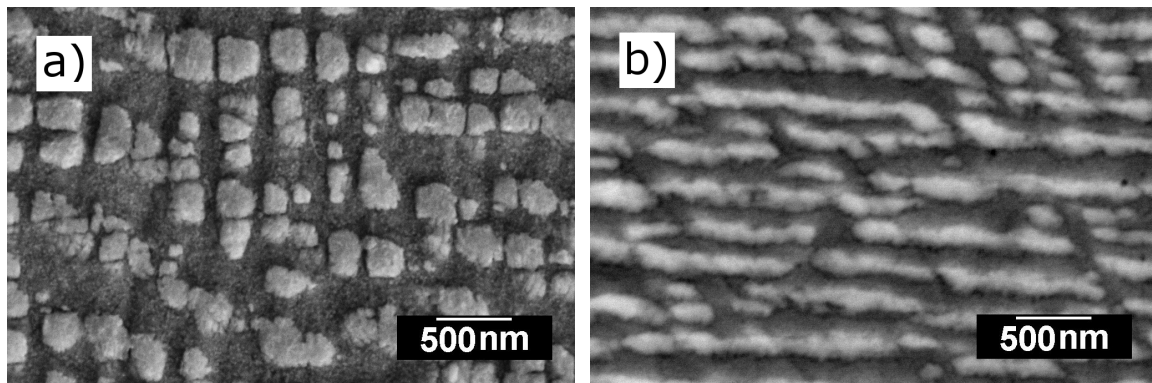

Figure 9: Microstructures of the alloys Co-9Al-9W-2Ti-0.12B, Co-9Al-9W-1Mo-0.04B, Co-9Al-9W-2Si and Co-9Al-9W-0.08B in aged condition (a-d) and after creep tests at 850 °C (e-l). Images are taken parallel e) - h) and perpendicular i) – l), respectively, to the applied stress axis. All micrographs in this figure have the same magnification.

Figure 10: TEM micrographs of the deformation structure in crept specimens of alloy 9W-0.12B. (a) and alloy 10W-2Nb (b) pictured along [001] direction in two beam case using the [200] reflection (both crept at 850 °C under final load of 450 MPa).

Figure 11: Microstructures of the alloy 9W-08B after creep tests at 950 °C. Image taken a) perpendicular b) parallel to the applied stress.
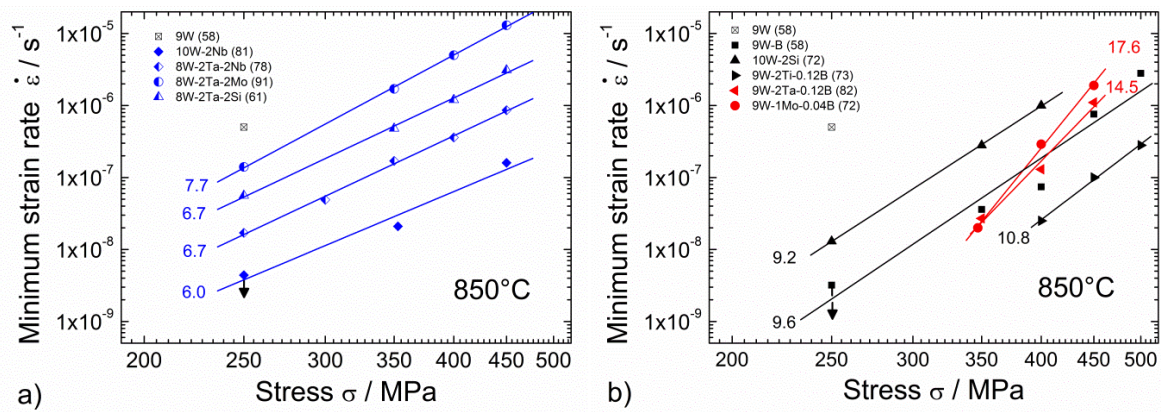
Figure 12: Norton-Plots of the creep experiments divided into groups according to the stress exponent n. a) Boron free alloys exhibiting intermetallic phases at the grain boundaries. b) Alloys exhibiting W-rich precipitates or W-rich borides at the grain boundary with the adjacent γ'-depleted zone.